*Ab initio* investigation of phonon modes in the $MgAl_2O_4$ spinel



2002 J. Phys.: Condens. Matter 14 3543

(http://iopscience.iop.org/0953-8984/14/13/312)

INSTITUTE OF PHYSICS PUBLISHING JOURNAL OF PHYSICS: CONDENSED MATTER

J. Phys.: Condens. Matter **14** (2002) 3543–3552 PII: S0953-8984(02)32730-9

# *Ab initio* investigation of phonon modes in the $MgAl_2O_4$ spinel

**Pascal Thibaudeau**[1] **and François Gervais**[2]

[1] Commissariat à l'Energie Atomique Le Ripault, BP 16, F-37260 Monts, France
[2] Laboratoire d'Electrodynamique des Matériaux Avancés, FRE2077 CNRS, LRCM01 CEA, Faculté des Sciences et Techniques, Université François Rabelais, Parc de Grandmont, F-37000 Tours, France

E-mail: Pascal.Thibaudeau@cea.fr

Received 15 January 2002, in final form 22 February 2002
Published 22 March 2002
Online at stacks.iop.org/JPhysCM/14/3543

**Abstract**

*Ab initio* infrared and Raman phonon modes in the normal cubic $MgAl_2O_4$ spinel are calculated at the first Brillouin zone centre using density functional theory with plane-wave basis and norm-conserving pseudopotentials. Good agreement with available experimental infrared and Raman spectra is found for both natural and synthetic spinel. A new set of infrared measurements on synthetic spinels shows extra vibrational infrared modes which are not predicted by calculations on normal spinel. The ionic character of spinels is illustrated by comparison between calculated and experimental Born effective charges.

## 1. Introduction

Spinel oxides form an important range of ceramic compounds with great interesting electrical, mechanical, magnetic and optical properties. It is observed that wide bandgaps in these structures offer attractive photoelectronic and optical applications [1]. Studies on spinel oxides also have numerous applications in geophysics and magnetism [2, 3]. For instance, the spinel transition of olivive, which is a major constituent of Earth's mantle, is widely accepted as the origin of the near 410 km seismic discontinuity [4]. Moreover, spinel oxides are found to be highly resistant to radiation-induced swelling and transformations at elevated temperatures [5, 6]. Magnesium dialuminium oxide ($MgAl_2O_4$) is often considered as a prototype of the $AB_2O_4$ family materials, which crystallizes in spinel structure [7].

Detailed analysis of the vibrational spectra of spinels, and especially in the case of $MgAl_2O_4$, is complicated by order/disorder phenomena that occur in such structures [8]. In normal spinel, an A divalent cation occupies one of the eight possible tetrahedral sites and a B trivalent cation is located in one of the 16 possible octahedral sites. Besides, tetrahedral and octahedral cationic exchange, giving rise to partially inverse spinels [9], is experimentally observed. Such changes in the cationic order are usually induced by high temperature and/or

  

high pressure. According to Navrotsky and Kleppa [10], one could characterize a two-species spinel oxide by an inversion or disorder parameter $x$ in such a way that the general formula $(A_{1-x}B_x)_{tet}[A_xB_{2-x}]_{oct}O_4$ can describe separately the tetrahedral and octahedral interstitial sites occupancies. The normal spinel is obviously found for $x = 0$ and the full inverse structure is given by $x = 1$.

From ambient to high temperatures, the disorder parameter is obtained from *in situ* neutron diffraction measurements [11]. However, due to the unquantified extent associated with the cation site exchanges [12, 13], it is difficult to describe properly the degree of short-range order and therefore to distinguish between different models of disorder. To complicate the interpretation even further, non-stoichiometric spinels $AO.yB_2O_3$ exist with $y > 1$ exhibiting cationic disorder and vacancies for both cationic sites [14, 15].

To quantify the nature and amplitude of disorder in synthetic spinels from vibrational spectra, a non-ambiguous normal mode assignment is required. Thus, an *ab initio* methodology is applied on normal $MgAl_2O_4$ spinel structure to clarify infrared and Raman spectroscopic interpretation. This interpretation is then discussed in the light of a new set of infrared reflectivity measurements on synthetic spinels.

## 2. Theoretical framework

### *2.1. Symmetry analysis*

It is now commonly accepted that normal spinel exhibits a cubic structure, with space group $Fd3m(\Theta_h^7)$ and 56 atoms per unit cell ($Z = 8$). Fourfold- (special 8a Wyckoff position) and eightfold- (special 16d Wyckoff position) coordinated cationic sites are located in an oxygen (general 32e Wyckoff position) close-packed pseudo-face-centred-cubic sublattice. To complete the description of the anion position, an additional parameter, generally labelled by $u$ and known in oxide spinels as the internal oxygen parameter, is introduced. In most spinels, $u$ lies between 0.24 and 0.275 if the origin of the unit cell is taken at the centre of inversion. For the particular value $u = 0.25$, the anions form an exactly cubic close-packed lattice and define a regular tetrahedron and octahedron with the cation as a centre. As $u$ increases, the oxygens move along the $\langle 111 \rangle$ direction, causing the tetrahedral site to enlarge at the expense of the octahedral one [16, 17].

Only two formula units are present in the primitive unit cell, leading to 42 normal modes. In addition to three acoustic modes of $T_{1u}$ symmetry, 39 optic modes are distributed among the following symmetries at the Brillouin zone centre:

$$\Gamma = A_{1g}(R) + E_g(R) + 3T_{2g}(R) + 4T_{1u}(IR) + T_{1g} + 2A_{2u} + 2E_u + 2T_{2u},$$

where R (IR) denotes Raman (infrared) activity and the remaining modes are silent [8, 18]. In a normal, non-defective $MgAl_2O_4$ spinel and without mode couplings, selection rules suggest that only five modes should be Raman active and four modes infrared active.

### *2.2. Ab initio methodology*

Powerful techniques were developed a few years ago to calculate vibrational properties of extended systems through density functional perturbation theory (DFPT) [19]. This theory allows self-consistent calculation of the linear response to an external perturbation in an extended system and combines the advantages of both the frozen phonon method [20–22] and the dielectric theory [23–25]. For the calculations of the electronic density response functions, it is necessary to obtain the wavefunction of the ground state only. Moreover, as there is no restriction to high-symmetry points as in the frozen phonon calculation, perturbations of

**Table 1.** Comparison between experimental and calculated lattice constant and oxygen parameter in the $MgAl_2O_4$ spinel. Relative errors are shown in parenthesis.

| | Experiment[a] | DFT all-electron | DFT-LDA-NCPP (this work) |
|---|---|---|---|
| Lattice constant (Å) | 8.060 | 8.072(+0.15%)[b]<br>8.056(−0.05%)[c] | 7.905(−1.9%) |
| Internal oxygen $u$ | 0.2624 | 0.2748(+4.7%)[b],<br>0.2638(+0.5%)[c] | 0.2735(+4.2%) |

[a] Extrapolated to $T = 0$.
[b] [37].
[c] [38].

arbitrary wavelength can be evaluated. These techniques have been successfully applied to the phonon dispersion curve of elemental and binary semiconductors [26], simple metals [27] and simple binary alkaline-earth oxides [28]. However, some phonon dispersion curves of more complex structures such as perovskites have been studied in the linear response approach within the framework of the linearized plane-wave (LAPW) method [29].

The ground state of $MgAl_2O_4$ spinel is calculated using density functional theory within the local density approximation (DFT-LDA) parametrized by Perdew and Wang [30]. A plane-wave basis set and norm-conserving pseudopotentials (NCPPs) for valence electrons only in the fully separable form given by Kleinman and Bylander [31] are used. From a scalar relativistic all-electron configuration, the pseudopotential generation follows the schemes proposed by Hamann [32] and by Troullier and Martins [33] for the cations and the oxygen respectively. Because it generates a smoother oxygen pseudopotential, the scheme derived by Troullier and Martins significantly reduces the computer memory consumption without having a noticeable effect on the results. Only linear core–valence correction is used in the generation of cationic pseudopotentials [34]. During their constructions, unphysical bound states or resonances appearing in the valence spectrum are ruled out by choosing suitable cutoff radii and local potential component as proposed by Gonze and co-workers [35]. The convergence of the pseudo-wavefunctions in momentum space is monitored to estimate a suitable basis set cutoff of 80 Ryd for the plane-wave calculations of all species. For the Brillouin zone sampling, a $4 \times 4 \times 4$ grid is used for the $k$-point summation in the self-consistent calculations [36], which leads to relatively unaffected structural parameters.

## 3. Computational results

### *3.1. Ground-state equilibrium properties*

During self-consistent cycles, the external pressure is kept fixed. The lattice parameter and oxygen internal position are optimized according to the symmetries of the cell until the internal forces and the stress are both close to zero. The values found are reported in table 1 for zero pressure.

The pressure is then varied and the previous process is repeated until the forces acting on atoms are close to zero and the diagonal components of the stress tensor are all equal to the external pressure. Both the internal energy and volume are collected in order to fit six different equations of state (EOS) at zero temperature. All these EOSs recover the previously optimized value of lattice parameter at zero pressure up to an absolute error of $10^{-4}$. To compare these calculated equilibrium properties, experimental lattice parameter and oxygen internal position are extrapolated to the zero-temperature limit from available data [39] obtained by neutron diffraction at different temperatures, neglecting the vibrational energy contribution.

**Table 2.** Calculated bulk modulus and its first derivative with respect to the pressure compared with experimental results in the $MgAl_2O_4$ spinel.

| | EOS | $K_0$ (GPa) | $K_0'$ |
|---|---|---|---|
| DFT-LDA-NCPP | Universal Tait [40] | 199 | 3.63 |
| (This work) | Born–Mie [41] | 198 | 3.56 |
| | [42] | 199 | 3.61 |
| | [43] | 199 | 3.60 |
| | [44] | 199 | 3.60 |
| | 3rd order | | |
| | [45] | 199 | 3.58 |
| DFT-LCAO | [46] | 227[a], 213[b] | 3.4[a], 5.4[b] |
| Experiments | | 196[c], 196[d], 196[e] | 4.89[c], 5.3[d], 4.7[e] |

[a] [38].
[b] [47].
[c] [48].
[d] [49].
[e] [50].

The fitting procedure on the EOSs allows us to obtain the bulk modulus $K_0$ and its first derivative with respect to the pressure $K_0'$ as a by-product. The values calculated are summarized in table 2 and, due to the relatively small pressure extent, no obvious effect is found with a particular choice of an EOS.

However, the lowest residual $\chi^2$ on fitted values is obtained using the Brennan–Stacey EOS. The equilibrium total energy versus density curve and the corresponding Brennan–Stacey EOS interpolation are reported in figure 1.

The lattice constant and oxygen position determined in this way are also compared with all-electron calculations. They are much more underestimated, essentially due to the linearity of the core–valence density imposed on generating cationic pseudopotentials [34]. For the same reason, the bulk modulus is slightly overestimated in the LDA compared with experiment as previously reported for other simple compounds [51] but agreement with experiments is still acceptable. Introduction of a nonlinear core–valence correction might possibly improve the results but it is out of the scope of the present paper.

### *3.2. Lattice dynamics at the Brillouin zone centre*

The *ab initio* vibrational frequencies at the zone centre are reported in table 3 and compared with calculated values using interatomic potentials [52]. The non-analytical part of the dynamical matrix is carefully taken into account using the full Born effective charge tensors to find the correct LO–TO splitting [53]. The overall agreement between available experimental data from table 3 and interatomic potentials is very good. However little discrepancy is found for the $E_g$ mode and one $T_{2g}$ Raman mode around 490 $cm^{-1}$. The Raman intensity of the predicted $T_{2g}$ Raman mode near 553 $cm^{-1}$ is probably very weak, which makes its precise experimental determination difficult.

As $MgAl_2O_4$ spinel is a known polar compound, the DFPT is a suitable theory which allows us to calculate the low- and high-frequency dielectric constants and the Born effective charge tensors directly on all inequivalent atoms [19]. The results are summarized in table 4. It is observed that the Born tensors are fully diagonal on cations and mainly diagonal on oxygen atoms up to $2 \times 10^{-2}$. The agreement between calculated and experimentally derived diagonal parts of the Born effective tensors is excellent.

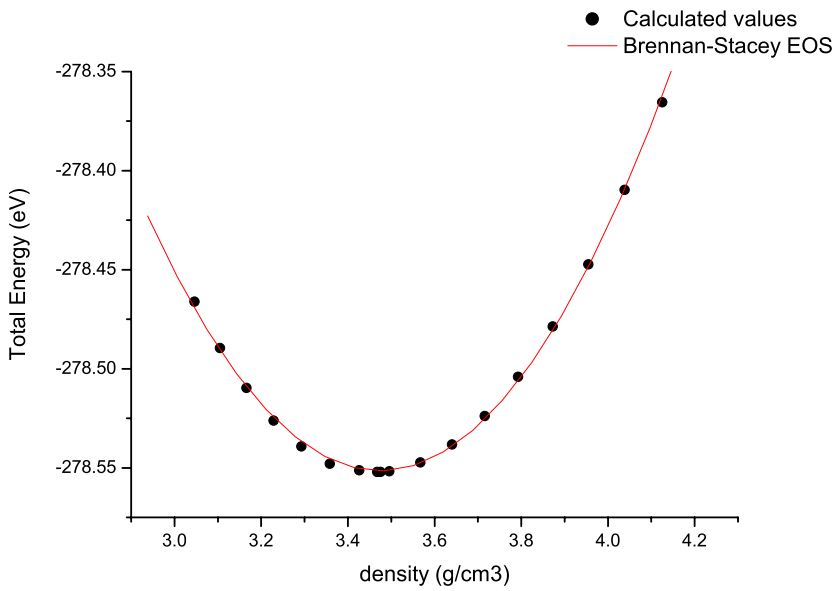


**Figure 1.** Calculated EOS of normal cubic $MgAl_2O_4$ fitted with a Brennan–Stacey form.

**Table 3.** DFT-LDA-NCPP vibrational frequencies in $cm^{-1}$ in the $MgAl_2O_4$ spinel compared with Lauwers and Herman results using interatomic potentials [52]. Relative errors are shown in parenthesis.

| | Vibrational frequencies ($cm^{-1}$) | |
|---|---|---|
| Symmetry | DFT-LDA-NCPP | Lauwers and Herman |
| $A_{1g}$(R) | 760 | 772(+2%) |
| $E_g$(R) | 380 | 403(+6%) |
| $T_{2g}$(R) | 309 | 281(−9%) |
| | 553 | 597(+%) |
| | 661 | 679(+3%) |
| $T_{1u}$(TO) | 307 | 337(+10%) |
| | 478 | 481(+1%) |
| | 565 | 497(−12%) |
| | 666 | 664(−0.3%) |
| $T_{1u}$(LO) | 309 | 337(+9%) |
| | 612 | 601(−2%) |
| | 564 | 488(−13%) |
| | 854 | 803(−6%) |
| $T_{2u}$ | 191 | |
| | 495 | |
| $T_{1g}$ | 315 | |
| $E_u$ | 392 | |
| | 602 | |
| $A_{2u}$ | 669 | |
| | 742 | |

The diagonal feature of the Born effective tensors is a direct consequence of the binding ionic character in the spinel. Even if each anion in that spinel is surrounded by three

**Table 4.** Calculated low- and high-frequency dielectric constants and Born effective charges compared with various experiments.

| | $\epsilon_0$ | $\epsilon_\infty$ | $Z_{\mathrm{Mg}}$ | $Z_{\mathrm{Al}}$ | $Z_{\mathrm{O}}$ |
|---|---|---|---|---|---|
| DFT-LDA-NCPP | 8.16 | 3.00 | 2.02 | 2.76 | −1.89 |
| Experiment | 8.16[a], 8.18–8.32[c] | 2.89–2.92[a], 2.93[b] | $2.1 \pm 0.4$[b] | $2.7 \pm 0.2$[b] | $-1.89 \pm 0.04$[b] |

[a] [54].
[b] This work.
[c] [55].

octahedrally coordinated cations of Al and one tetrahedrally coordinated cation of Mg, the effective field is mainly isotropic. Based on these *ab initio* Born charge calculations, an ionic model using simple interatomic potentials should be able to accurately reproduce the main features of the vibrational spectrum at the zone centre [56]. The calculated dielectric constants are slightly overestimated by LDA to the order of several per cent but remain compatible with experiments. These overestimated values are due to the fact that LDA is widely based on the electron-gas approximation and its exchange–correlation form has a 'memory' of its metallic parentage [57].

## 4. Reflectivity measurements

It is a difficult task to interpret precisely the vibrational modes of $MgAl_2O_4$ in the $Fd3m$ structure [8]. Table 5 summarizes experimental infrared and Raman vibrational frequencies for $MgAl_2O_4$ collected over the past 30 years.

Obviously, frequencies are affected by the true nature of the measured sample and many authors have tried to resolve this difficulty by comparing differently prepared samples [58]. Cationic disorder lowers the symmetry and increases available vibrational modes. As the cationic masses and total electronic charges are close in $MgAl_2O_4$, slight differences in disordered spinel spectra are observed. Only recently, an experimentally induced disorder Raman mode has been interpreted unambiguously [6].

Indeed, the availability of Fourier-transform infrared spectroscopy justifies remeasuring the reflectivity of the $MgAl_2O_4$ single crystal because resolution, spectral accuracy and sensitivity have been significantly improved with respect to earlier experiments. New measurements are carried out on two different synthetic spinel single crystals from MTI Corp, grown by the Czochralski method with two optically polished and oriented sides along the $\langle 100 \rangle$ lattice direction. The reflectivity spectra at normal incidence are collected on a Bruker IFS66v infrared Fourier spectrometer. The general results agree within experimental error with previously published spectra [54, 59, 67]. However, the very weak infrared band near 227 $\mathrm{cm}^{-1}$, which is absent from previous infrared reports, is unambiguously observed in both spectra. This mode is consistent with the extra modes observed by Raman scattering as shown in table 5. It may be assigned to vibration induced by an exchange between Mg and Al sites or to the defective nature of the non-stoichiometric spinel lattice [69]. This particular point will be the subject of a forthcoming paper. The complex dielectric function at the zone centre is expressed in the form of the generalized Lyddane–Sachs–Teller relationship, first proposed by Kurosawa [61] as

$$\varepsilon(\omega) = \varepsilon_\infty \prod_{j=1}^{n_{IR}} \frac{\omega_j^2(\mathrm{LO}) - \omega^2 - \imath\Gamma_j(\mathrm{LO})\omega}{\omega_j^2(\mathrm{TO}) - \omega^2 - \imath\Gamma_j(\mathrm{TO})\omega}, \tag{1}$$

where the $\omega_j$ and $\Gamma_j$ stand for the phonon mode frequencies and dampings respectively. TO and LO suffixes refer to optically transverse and longitudinal modes respectively. Equation (1)

**Table 5.** Reported experimental vibrational frequencies in $cm^{-1}$, including the frequencies and damping measurements from synthetic spinels obtained in this work.

| Reference | $A_{1g}$(R) | $E_g$(R) | $T_{2g}$(R) | | | $T_{1u}$(IR) | | | | Others |
|---|---|---|---|---|---|---|---|---|---|---|
| [66] | | 410 | 311 | 492 | 611 | 305[a] | 428[a] | 485[a] | 670[a] | 722($A_{1g}$) |
| | | | | | | 311[b] | | 497[b] | 800[b] | |
| [6, 58] | 770 | 409 | 311 | | 670 | | | | | |
| [18] | 767 | 407 | 312 | | 666 | 304[a] | 476[a] | 578[a] | 676[a] | 800(IR) |
| | | | | | | 312[b] | 610[b] | 575[b] | 868[b] | |
| [15] | 769 | 410 | 310 | 490 | 668 | 308[a] | 494[a] | 569[a] | 676[a] | 223(R) |
| | | | | | | 313[b] | 609[b] | 570[b] | 878[b] | 725($A_{1g}$) |
| [67] | | | | | | 306[a] | 490[a] | 580[a] | 670[a] | |
| | | | | | | 312[b] | 609[b] | 610[b] | 857[b] | |
| [68] | 770 | 405 | 305 | 485 | 663 | | | | | 225(R) |
| [69] | 772 | 410 | 311 | 492 | 671 | 305[a] | 428[a] | 485[a] | 670[a] | 727($A_{1g}$) |
| | | | | | | | | 630[b] | 855[b] | |
| [70] | | | | | | 309[a] | 522[a] | 580[a] | 688[a] | |
| Frequencies ($cm^{-1}$) | | | | | | 303[a] | 491[a] | 532[a] | 675[a] | 226[a](IR) |
| this work | | | | | | | | | | 805[a](IR) |
| | | | | | | 307[b] | 608[b] | 532[b] | 870[b] | 227[b](IR) |
| | | | | | | | | | | 796[b](IR) |
| Dampings ($cm^{-1}$) | | | | | | 18[a] | 43[a] | 44[a] | 42[a] | 14[a] |
| this work | | | | | | | | | | 74[a] |
| | | | | | | 23[b] | 58[b] | 54[b] | 42[b] | 15[b] |
| | | | | | | | | | | 68[b] |

[a] Transverse mode.
[b] Longitudinal mode.

is then combined with the Fresnel formula for reflectivity of a half-space medium near normal incidence with vacuum as reference

$$R(\omega) = \left| \frac{\sqrt{\varepsilon(\omega)} - 1}{\sqrt{\varepsilon(\omega)} + 1} \right|^2. \tag{2}$$

The high-frequency dielectric constant, phonon modes and dampings are then fitted from reflectivity data. An excellent agreement can be achieved as illustrated in figure 2.

Data fit parameters are compared with previous reported data in table 5. Such a combination of infrared Fourier spectrometry and data fitting allows the determination of polar phonon frequencies that are relevant in equation (1), with a precision better than 0.5%. Large dampings are found for two intense infrared modes. These large dampings associated with intense modes may be interpreted as a consequence of the grit finish as previously reported on $Al_2O_3$ corundum by Barker [60]. The complex index is then deduced using equation (1) combined with $\varepsilon = n^2$ and the parameters which yield the best fit to reflectivity data. The results obtained with this technique are consistent with a direct Kramers–Krönig transformation on reflectivity data.

To deduce the effective charges from measurements, a relationship proposed by Kurosawa [61] and later exploited in many compounds, mainly oxides [62–65], was used. This relation shows, still within the context of a quasi-harmonic vibrational model, that the Born effective charge $Ze$ (where $e$ is the electron charge) in a spherical isotropic effective field is related to TO and LO phonon frequencies via

$$\sum_{j=1}^{n_{IR}} (\omega_j^2(\mathrm{LO}) - \omega_j^2(\mathrm{TO})) = \frac{1}{\varepsilon_0 V} \sum_{k=1}^{n_{atom}} \frac{Z_k^2 e^2}{m_k}, \tag{3}$$

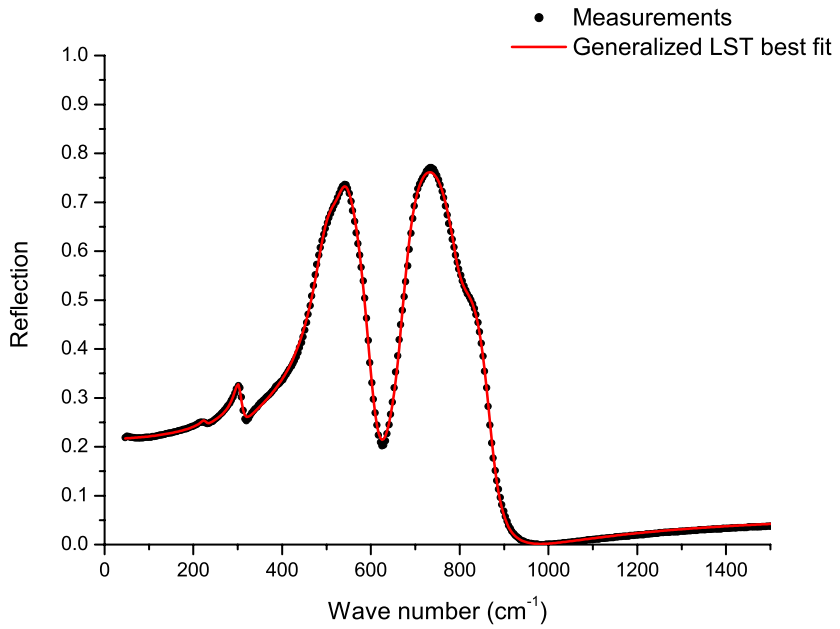


**Figure 2.** Infrared reflectivity measurements and generalized Lyddane–Sachs–Teller best fitted values in the cubic $MgAl_2O_4$ spinel.

where the summation in the right-hand side of the equation is over all atoms of mass $m_k$ contained in the unit cell of volume $V$ and the summation in the left-hand side of the equation is over all IR-active modes. $\varepsilon_0$ is the vacuum dielectric constant. Equation (3) and the charge neutrality condition are available to determine the three Born effective charges. Therefore a realistic value for one of the cationic effective charges is required to deduce the two others. The procedure is repeated until a satisfactory effective charge set is found [15]. The oxygen effective charge is not very sensitive to the various choices of cationic charges because of the weight of the oxygen atom in equation (3). Due to the relative uncertainty of the experimental frequencies, the cationic charges may balance each other, as illustrated in table 4.

Better values of Born effective charges are found if both TO and LO infrared frequencies are correctly determined. Some authors have tried to calculate these frequencies by molecular mechanics using interatomic potentials [15, 16, 52]. Unfortunately, these potentials are often fitted on spinel experimental data, including vibrational frequencies, but frequency data themselves are often insufficient to determine accurate interatomic potentials and a full analysis on a given single crystal is not always possible.

The measured effective charge on oxygen atoms is close to the value previously found by Ishii and co-workers [15] and previously found by Gervais [63] on aluminium atoms in $Al_2O_3$. However, the values calculated by Ishii on cations are different from both the present measurements and the *ab initio* calculations. These discrepancies may be due to a lack of precision in their frequency determination.

## 5. Conclusion

Structural properties in the normal cubic $MgAl_2O_4$ spinel were calculated using DFT with plane-wave basis and pseudopotentials. A DFPT vibrational mode analysis on the previously

calculated ground state was performed in order to give new insights into the interpretation of infrared and Raman spectroscopic measurements. Conclusive agreement is found for both structural and vibrational properties in the normal non-defective cubic $MgAl_2O_4$ spinel. A new set of infrared measurements on synthetic spinels shows modes which are forbidden by group theory for normal spinel. These infrared modes around 227 and 806 $cm^{-1}$ could originate in the defective nature of the spinel lattice. Calculated Raman modes on normal spinel are shown to be useful to investigate the vibrational spectrum differences on synthetic spinels, demonstrating that the Raman mode near 725 $cm^{-1}$ of $A_{1g}$ character is not a harmonic natural spinel mode as experimentally observed by Cynn and co-workers [6]. Detailed analysis between calculated and measured Born effective charges suggests no significant differences between normal and synthetic spinel samples. It is shown that, even on the anion, the ionic character of binding in this spinel is recovered by the diagonal feature of the calculated Born effective tensors.

## Acknowledgment

One of the authors (PT) would like to express special thanks to S Labayle-Camus for helpful discussions.

## References

[1] Ueda N, Omata T, Hikuma N, Ueda K, Mizoquchi H, Hashimoto T and Kawazoe H 1992 *Appl. Phys. Lett.* **61** 1954
[2] Green H W II 1984 *Geophys. Res. Lett.* **11** 817
[3] Schiessl W *et al* 1996 *Phys. Rev.* B **53** 9143
[4] Ringwood A E and Major A 1970 *Phys. Earth Planet. Inter.* **3** 89
[5] Cain L S, Pogatshnik G J and Chen Y 1988 *Phys. Rev.* B **37** 2645
[6] Cynn H, Sharma S K, Cooney T F and Nicol M 1992 *Phys. Rev.* B **45** 500
[7] Galasso F S 1970 *Structure and Properties of Inorganic Solids* (New York: Pergamon)
[8] White W B and DeAngelis B A 1967 *Spectrochim. Acta* A **23** 985
[9] Schmoker U, Boesch H R and Waldner F 1972 *Phys. Lett.* A **40** 237
[10] Navrotsky A and Kleppa O J 1967 *J. Inorg. Nucl. Chem.* **29** 2701
[11] Redfern S A T, Harrison R J, O'Neill H St C and Wood D R R 1999 *Am. Mineral.* **84** 299
[12] Wood B J, Kirkpatrick R J and Montez B 1986 *Am. Mineral.* **71** 999
[13] O'Neill H St C and Navrotsky A 1983 *Am. Mineral.* **68** 181
[14] Dupree R, Lewis M H and Smith M E 1986 *Phil. Mag.* A **53** L17
[15] Ishii M, Hiraishi J and Yamanaka T 1982 *Phys. Chem. Minerals* **8** 64
[16] Striefler M E and Barsch G R 1972 *J. Phys. Chem. Solids* **33** 2229
[17] Hill R J, Craig J R and Gibbs G V 1979 *Phys. Chem. Minerals* **4** 317
[18] Chopelas A and Hofmeister A M 1991 *Phys. Chem. Minerals* **18** 279
[19] Baroni S, Giannozzi P and Testa A 1987 *Phys. Rev. Lett.* **58** 1861
[20] Wendel H and Martin R M 1979 *Phys. Rev.* B **19** 5251
[21] Kunc K and Martin R M 1982 *Phys. Rev. Lett.* **48** 406
[22] Yin M T and Cohen M L 1982 *Phys. Rev.* B **26** 3259
[23] Sham L J 1969 *Phys. Rev.* **188** 1431
[24] Pick P, Cohen M H and Martin R M 1970 *Phys. Rev.* B **1** 910
[25] Falter C 1988 *Phys. Rep.* **164** 1
[26] Giannozzi P, de Gironcoli S, Pavone P and Baroni S 1991 *Phys. Rev.* B **43** 7231
[27] de Gironcoli S 1995 *Phys. Rev.* B **51** 6773
[28] Schütt O, Pavone P, Windl W, Karch K and Strauch D 1994 *Phys. Rev.* B **50** 3746
[29] Yu R and Krakauer H 1995 *Phys. Rev. Lett.* **74** 4067
[30] Perdew J P and Wang Y 1992 *Phys. Rev.* B **45** 13 244
[31] Kleinman L and Bylander D M 1982 *Phys. Rev. Lett.* **48** 1425
[32] Hamann D R 1989 *Phys. Rev.* B **40** 2980
[33] Troullier N and Martins J L 1991 *Phys. Rev.* B **43** 1993

[34] Louie S G, Froyen S and Cohen M L 1982 *Phys. Rev.* B **26** 1738
[35] Gonze X, Stumpf R and Scheffler M 1991 *Phys. Rev.* B **44** 8503
[36] Monkhorst H J and Pack J D 1976 *Phys. Rev.* B **13** 5188
[37] Wei S H and Zhang S B 2001 *Phys. Rev.* B **63** 045112
[38] Catti M, Valerio G, Dovesi R and Causà M 1994 *Phys. Rev.* B **49** 14 179
[39] Fischer P 1967 *W. Kristallogr.* **124** 275
[40] MacDonald J R 1969 *Rev. Mod. Phys.* **38** 669
MacDonald J R 1969 *Rev. Mod. Phys.* **41** 316
[41] Anderson O L 1995 *Equations of State of Solids for Geophysics and Ceramic Science* (New York: Oxford University Press)
[42] Brennan B J and Stacey F D 1979 *J. Geophys. Res.* **84** 5535
[43] Vinet P, Ferrante J, Smith J R and Rose J H 1987 *Phys. Rev.* B **35** 1945
[44] Shanker J, Kushwah S S and Kumar P 1997 *Physica* B **239** 337
[45] Birch F 1986 *J. Geophys. Res.* **91** 4949
[46] Murnaghan F D 1944 *Proc. Natl Acad. Sci. USA* **30** 244
[47] Mo S D and Ching W Y 1996 *Phys. Rev.* B **54** 16 555
[48] Chang Z P and Barsch G R 1973 *J. Geophys. Res.* **78** 2418
[49] Yoneda A 1990 *J. Phys. Earth* **38** 19
[50] Kruger M B, Nguyen J H, Caldwell W and Jeanloz R 1997 *Phys. Rev.* B **56** 1
[51] Fuchs M, Bockstedte M, Pehlke E and Scheffler M 1998 *Phys. Rev.* B **57** 2134
[52] Lauwers H A and Herman M A 1980 *J. Phys. Chem. Solids* **41** 223
[53] Gonze X and Lee C 1997 *Phys. Rev.* B **55** 10 355
[54] Palik E D (ed) 1991 *Handbook of Optical Constants of Solids* vol 2 (London: Academic)
[55] Shannon R D and Rossman G R 1991 *J. Phys. Chem. Solids* **52** 1055
[56] Thibaudeau P and Da Rocha S, in preparation
[57] Baroni S and Resta R 1986 *Phys. Rev.* B **33** 7017
[58] Cynn H, Anderson O L and Nicol N 1993 *Pure Appl. Geophys. (PAGEOPH)* **141** 415
[59] McMillan P F and Hofmeister A M 1988 *Rev. Mineral.* **18** 99
[60] Barker A S 1963 *Phys. Rev.* **132** 1474
[61] Kurosawa T J 1961 *J. Phys. Soc. Japan* **16** 1298
[62] Scott J F 1971 *Phys. Rev.* B **4** 1360
[63] Gervais F 1976 *Solid State Commun.* **18** 191
[64] Gervais F and Arend H 1983 *Z. Phys.* B **50** 17
[65] Gervais F and Kaczmarek W 1983 *Z. Phys.* B **51** 137
[66] Tropf W J, Thomas M E and Haris T J 1995 Properties of crystals and glasses *Handbook of Optics, Devises, Measurements and Properties* 2nd edn, vol 2, ed M Bass, E W Van Stryland, D R Williams and W L Wolfe (New York: McGraw-Hill) ch 33
[67] Striefler M E and Boldish S I 1978 *J. Phys. C: Solid State Phys.* **11** L237
[68] Fraas L M, Moore J E and Salzberg J B 1973 *J. Chem. Phys.* **58** 3585
[69] O'Horo M P, Frisillo A L and White W B 1973 *J. Phys. Chem. Solids* **34** 23
[70] Preudhomme J and Tarte P 1971 *Spectrochim. Acta* A **27** 1817